

# Pit formation on poly(methyl methacrylate) due to ablation induced by individual slow highly charged ion impact

R. RITTER<sup>1</sup>, R. A. WILHELM<sup>2</sup>, R. GINZEL<sup>3</sup>, G. KOWARIK<sup>1</sup>, R. HELLER<sup>2</sup>, A. S. EL-SAID<sup>2</sup>, R. M. PAPALÉO<sup>4</sup>, W. RUPP<sup>5</sup>, J. R. CRESPO LÓPEZ-URRUTIA<sup>3</sup>, J. ULLRICH<sup>3</sup>, S. FACSKO<sup>2</sup> and F. AUMAYR<sup>1(a)</sup>

<sup>1</sup> *Institute of Applied Physics, TU Wien - 1040 Vienna, Austria, EU*

<sup>2</sup> *Institute of Ion Beam Physics & Materials Research, Helmholtz-Zentrum Dresden-Rossendorf 01328 Dresden, Germany, EU*

<sup>3</sup> *Max-Planck-Institut für Kernphysik - 69029 Heidelberg, Germany, EU*

<sup>4</sup> *Faculty of Physics, Catholic University of Rio Grande do Sul - 90619-900 Porto Alegre, Brazil*

<sup>5</sup> *IMS Nanofabrication AG - 1020 Vienna, Austria, EU*

received 29 September 2011; accepted in final form 17 November 2011

published online 3 January 2012

PACS 34.35.+a – Interactions of atoms and molecules with surfaces

PACS 79.20.-m – Impact phenomena (including electron spectra and sputtering)

PACS 68.49.Sf – Ion scattering from surfaces (charge transfer, sputtering, SIMS)

**Abstract** – We report the formation of nano-sized pits on poly(methyl methacrylate) after exposure to slow highly charged ion beams. The pits are formed on the polymer surface as a direct result of individual ion impacts. Intermittent contact mode atomic-force microscopy was employed to study the size evolution of the pits in dependence of potential and kinetic energies of the incident ions. A potential energy threshold value of approximately 7 keV was found for pit formation. Above this value an increase in potential energy results in an increasing pit volume, while the pit shape can be tuned by varying the kinetic energy.

Copyright © EPLA, 2012

**Introduction.** – Controlled and reproducible creation and manipulation of nano-sized objects in all three spatial directions are prominent goals in modern nanotechnology. Recently it has been demonstrated, that individual slow (keV) highly charged ions (HCI) are able to produce nano-sized structural modifications on various substrate surfaces by ion impact (see [1,2] and references therein). As the main reason for nanostructure formation, the localized deposition of their large amount of potential energy (*i.e.* sum of binding energy of all missing electrons) was identified [1]. The nature and appearance of such HCI-induced nanostructures depend heavily on the target material properties and the involved interaction processes and can range from hillocks (CaF<sub>2</sub> [1], SrTiO<sub>3</sub> [3]) and pits or craters (KBr [4], Si [5]) to caldera-type structures (TiO<sub>2</sub> [6]) and erasable regions of enhanced friction (HOPG [7], mica [8]). Similar surface modifications have been reported earlier as a result of individual-swift (MeV–GeV) heavy-ion impact [9–12]. However, these nanostructures on the surface are always coupled with radiation damage deep inside the bulk material (ion

tracks). This is not the case for slow HCI impact due to the extremely local nature of their potential energy deposition, thus making HCI a promising tool for more gentle nanostructuring in future applications.

In this letter we present studies of nano-sized surface modifications induced by the impact of individual slow highly charged ions on poly(methyl methacrylate) (PMMA), a polymer material commonly used in the semiconductor industry due to its role as a positive resist material under UV-light, X-ray, electron and ion irradiation. PMMA has been subject to a multitude of studies probing the materials response to ion beam treatment. MeV proton beam writing has been used to fabricate sub-surface cavities [13] and three-dimensional nanostructures [14] after the development of the exposed damage zone in a chemical bath. Features of (8–10) nm in size have been milled into thin films by means of a 50 keV Ga<sup>+</sup> focused ion beam [15]. Individual-swift heavy ions [16] and C<sub>60</sub> clusters [17] have been shown to produce etchable tracks tens of nanometers in diameter in the material, while direct cratering and ridge formation with a strong dependence on the initial charge state has been reported for the impact of single 3 MeV/amu Au ions [18]. Plasma

<sup>(a)</sup>E-mail: aumayr@iap.tuwien.ac.at

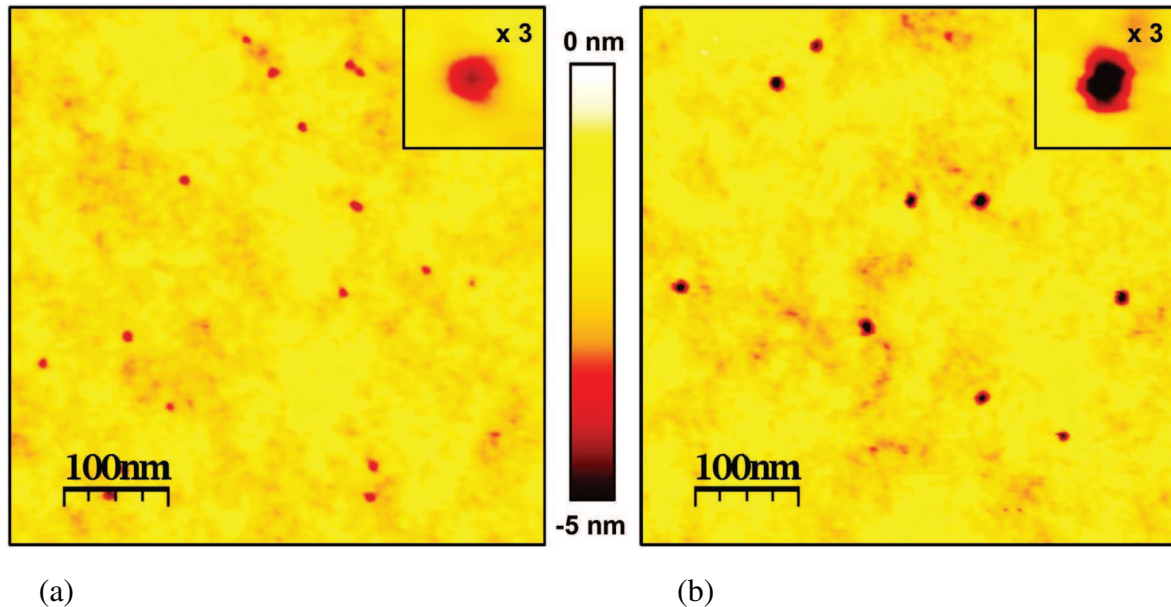


Fig. 1: (Color online) Intermittent contact mode AFM images of pits induced by individual impacts of  $\text{Xe}^{36+}$  ( $E_{\text{kin}} = 360$  keV, left) and  $\text{Xe}^{48+}$  ( $E_{\text{kin}} = 480$  keV, right) ions on PMMA. The insets show one individual pit for both cases at triple magnification.

treatment has been successfully employed to tune optical properties such as reflectivity [19], refractive index and extinction coefficient [20], or to induce a transition from hydrophilic to super-hydrophobic surfaces [19,21]. The only study with slow (keV) highly charged ions, to our knowledge, was conducted by Gillaspay *et al.* [22]. PMMA samples were irradiated with  $\text{Xe}^{44+}$  ( $E_{\text{kin}} = 210$  keV) ions under normal incidence through a nickel stencil mask at varying doses corresponding to complete exposure of the unmasked areas or single-ion impacts. In both cases, contrary to our findings, ion-induced structures could only be found after etching with a chemical developer.

**Materials and methods.** – For our studies PMMA targets were prepared at IMS Nanofabrication AG in Vienna by spin coating films of 45 nm thickness onto polished Si wafer substrates. Samples were irradiated with highly charged Xe and Bi ions extracted from electron beam ion traps (EBITs) at Helmholtz-Zentrum Dresden-Rossendorf and at Max Planck Institute for Nuclear Physics in Heidelberg.  $\text{Xe}^{q+}$  ions in charge states  $q = 12\text{--}40$  were delivered from a Dresden EBIT [23]. After charge state separation the ions could be decelerated by means of a two-stage deceleration lens system, the final impact energies on the surface ranging from 70–1400 eV/amu. The beam spot was scanned under normal incidence over an area of  $4 \times 4$  mm<sup>2</sup> on the target at typical fluences of  $5 \times 10^9$  cm<sup>-2</sup>.  $\text{Xe}^{36+}$ ,  $\text{Xe}^{48+}$  and  $\text{Bi}^{62+}$  ions were extracted from the Heidelberg EBIT [24], also equipped with a deceleration system [25]. Samples were irradiated under normal incidence with beam spots of 1.5–2 mm diameter at typical fluences of  $2 \times 10^9$  cm<sup>-2</sup> in a kinetic energy range of 300–3720 eV/amu. After

irradiation the surface topology of the samples was investigated without any further treatment at TU Wien with an MFP-3D atomic-force microscope (AFM) from Asylum Research operated with commercially available silicon cantilevers (Olympus, 7 nm nominal tip radius) in intermittent contact mode under ambient conditions. The samples were transported from the irradiation facilities to the AFM in regular sample holders (no vacuum conditions), as preliminary investigations had shown that exposure to air does not affect the appearance of the surface topology and the defects in AFM imaging, even after long storage times. The WSXM software [26] was used to display and analyse the obtained AFM images.

**Experimental results.** – In fig. 1, two examples for typical intermittent contact mode images of the PMMA surface after ion bombardment are depicted for comparison. Nano-sized pits or craters are clearly visible as a result of HCI impact. The respective number densities of pits in the AFM images are in good agreement with the applied ion fluences, *i.e.* basically every individual ion produces one single pit. Pits on the left-hand side induced by  $\text{Xe}^{36+}$  ions ( $E_{\text{pot}} = 27.8$  keV,  $E_{\text{kin}} = 360$  keV) are visibly slimmer and less deep than pits induced by  $\text{Xe}^{48+}$  ions ( $E_{\text{pot}} = 83.2$  keV,  $E_{\text{kin}} = 480$  keV). It is well known that PMMA behaves as a positive resist under energetic photon and particle bombardment [27] at low fluences due to the high yield of scissions created in the polymer chains. As our samples were not treated with a chemical developer prior to AFM imaging, we therefore suspect that the observed pits are the result of direct ablation of volatile reaction products formed after the initial ion-induced chain scissioning [13–18].

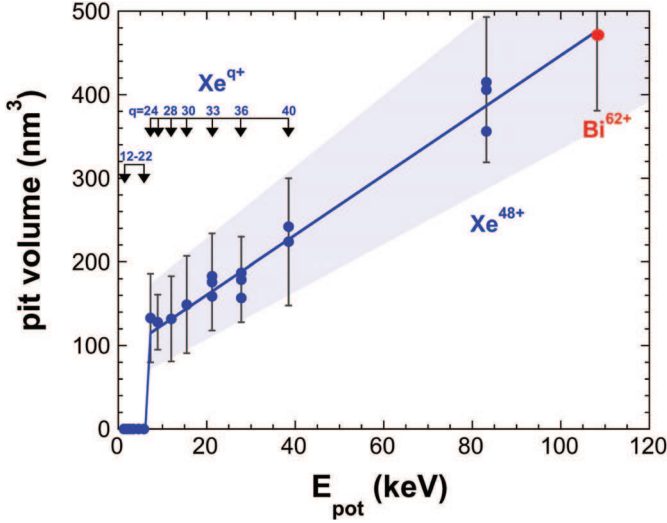


Fig. 2: (Color online) Evolution of the pit volume on PMMA as a function of the potential energy (charge state) of the incident ions. Multiple data points at a fixed potential energy correspond to measurements performed at different kinetic energies.

For each combination of potential and kinetic energy a minimum of 80 pits was analysed. Summarized data are displayed in fig. 2. Above a threshold value of approximately 7 keV ( $\text{Xe}^{24+}$ ), a linear increase in pit volume with increasing potential energy is found, whereas for charge states below this threshold ( $\text{Xe}^{12+}$ – $\text{Xe}^{22+}$ ) no visible pits are formed on the surface (or are no longer resolvable by our AFM). For a number of charge states, irradiations were performed at different kinetic energies (typically in the range of  $300 \text{ eV} \times q$ – $10 \text{ keV} \times q$ ), shown as multiple data points in fig. 2 at fixed potential energy and resulting in pits of comparable average volume. The error bars in fig. 2 display the fluctuations in pit size due to the statistical nature of the energy dissipation and the subsequent ablation process and not the errors of our AFM evaluation, which are lower. Such fluctuations are visible in every single AFM image (see fig. 1) and thus cannot result from using tips of varying shape and quality. To minimize variations indeed caused by differing AFM tip quality, every new tip was scanned over a reference sample with the deepest pits found and rejected if unable to adequately resolve these pits. In fig. 3, the influence of a variation in kinetic energy for a fixed ion species ( $\text{Xe}^{48+}$ ) is shown. While such a variation has very little impact on the total volume removed due to the ion impact for the three cases shown, an influence on the individual pit dimensions is apparent. In the high-energy case (480 keV, right inset) a much narrower and deeper pit is formed than in the low-energy case (43.2 keV, left inset). Simulations, which calculate the energy density deposited into a  $\text{CaF}_2$  surface by  $\text{Xe}^{33+}$  ions of largely different impact energies (5 keV *vs.* 330 keV; see fig. 4 in ref. [1]), show a remarkable similarity to the pit profiles found in our case (fig. 3). This behaviour with kinetic energy is not limited to  $\text{Xe}^{48+}$  but was also found

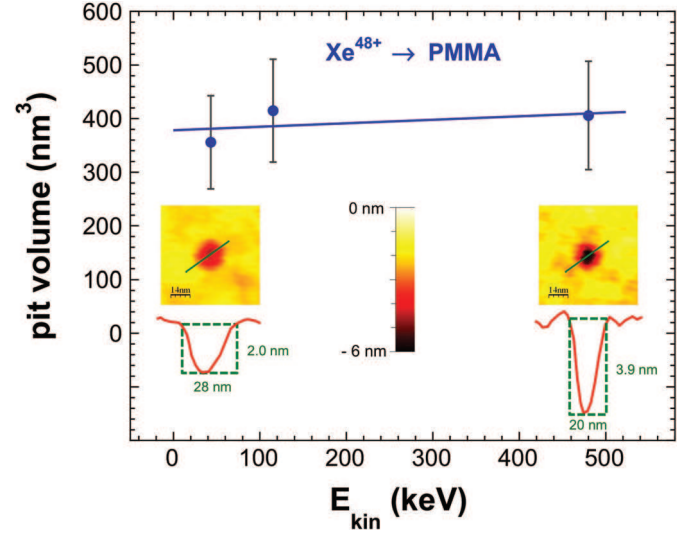


Fig. 3: (Color online) Evolution of the pit volume on PMMA for  $\text{Xe}^{48+}$  impact at varying kinetic energies. The insets show AFM images and depth profiles of one individual pit for the lowest energy (43.2 keV, left) and the highest energy (480 keV, right).

for other projectile charge states. Due to the fact that a feature of considerably smaller diameter (20 nm *vs.* 28 nm) shows a depth almost twice as large (3.9 nm *vs.* 2.0 nm) in the AFM measurement, we are confident that the depth measurement is not strongly influenced by the shape of the employed AFM tips. In our measurements the sharpest pit has an aspect ratio (depth/diameter) of about 1/5. Assuming a spherical tip, we should be able to resolve any pit structure, whose aspect ratio is smaller than that of our tip, *i.e.*  $r/2r = \frac{1}{2}$ , as long as the tip diameter is smaller than the diameter of the pit.

**Discussion and conclusions.** – From our data it becomes clear that (a) the nano-sized pits can unambiguously be associated to individual ion impact events, while many impacts of singly charged ions or electrons would be required to achieve the same; (b) in contrast to conventional electron or ion beam lithography, with HCI as projectiles there is no need of etching the damage zone by a chemical developer; (c) these pits occur above a certain potential energy threshold (*i.e.* minimum HCI charge state); (d) the volume of these pits increases linearly with the potential energy of the incident ions, while a variation in kinetic energy shows little influence on the overall pit volume; and (e) the pit shape can be tuned by varying the kinetic energy, *i.e.* a faster ion leaves behind a slimmer and deeper crater as compared to a slower ion of the same charge state.

To explain our findings we start with the well-known interaction scenario for the impact of slow HCI on surfaces (see, *e.g.*, [28–31] and references therein). The approaching HCI undergoes a large number of neutralization and de-excitation processes, by which many electrons from the target are transferred into highly excited states of the

projectile (“hollow-atom” formation), and subsequently emitted via auto-ionisation and other Auger processes [30]. Transfer of electrons to the projectile leaves unbalanced holes in the surface, thus structurally weakening the target. The Auger decay of the hollow atom leads to the emission of electrons with low to intermediate energies up to a few hundred eV [28]. For a HCI with  $q=40$  we estimate about 250 holes created in the course of the interaction of a single ion, accompanied by the very localized emission of more than 200 primary electrons followed by secondary-electron multiplication close to the impact point [32,33]. The potential energy stored in the incoming HCI will thus be deposited in the form of many holes and electron-hole pairs along the first few nm of its trajectory below the target surface. The kinetic energy of the projectile determines the depth within which the de-excitation of the projectile is completed. Quantitative simulations carried out for a CaF<sub>2</sub> single crystal show that this depth corresponds to  $\sim 1$  nm for 150 q eV and to  $\sim 4$  nm for 10 q keV Xe<sup>q+</sup> projectiles (see fig. 4 of [1]). In regions where the ionisation density responsible for polymer bond scission surpasses a certain critical value (threshold), polymer molecules or fragments are no longer bound and can be ejected or desorbed from the target surface. The proportionality of the average crater volume with HCI potential energy, the change in shape of the craters with kinetic energy, and even the existence of a threshold as seen in fig. 2 can thus be understood at least qualitatively. Below the threshold the number of broken bonds is not sufficient for the target material to be fully removed from the surface. The impact region is, however, structurally weakened and should be attackable by a suitable etchant [34]. Preliminary etching investigations indeed show that, for ions below the observed threshold (we have, *e.g.*, tried Xe<sup>22+</sup> and Xe<sup>20+</sup>), the individual impact regions can be revealed by etching the samples in isopropyl alcohol. Systematic etching investigations are therefore currently in progress.

\*\*\*

RR is a recipient of a DOC-fellowship of the Austrian Academy of Sciences. This work has been supported by the European Community as an Integrating Activity “Support of Public and Industrial Research Using Ion Beam Technology (SPIRIT)” under EC contract No. 227012. Support from the EU-network ITS-LEIF and the Austrian FWF (P17449) is acknowledged.

## REFERENCES

- [1] EL-SAID A. S., HELLER R., MEISSL W., RITTER R., FACSKO S., LEMELL C., SOLLEDER B., GEBESHUBER I. C., BETZ G., TOULEMONDE M., MOLLER W., BURGDORFER J. and AUMAYR F., *Phys. Rev. Lett.*, **100** (2008) 237601.
- [2] AUMAYR F., EL-SAID A. S. and MEISSL W., *Nucl. Instrum. Methods Phys. Res. B*, **266** (2008) 2729.
- [3] PETERS T., HAAKE C., HOPSTER J., SOKOLOVSKY V., WUCHER A. and SCHLEBERGER M., *Nucl. Instrum. Methods Phys. Res. B*, **267** (2009) 687.
- [4] HELLER R., FACSKO S., WILHELM R. A. and MOLLER W., *Phys. Rev. Lett.*, **101** (2008) 096102.
- [5] TONA M., WATANABE H., TAKAHASHI S., NAKAMURA N., YOSHIYASU N., SAKURAI M., TERUI T., MASHIKO S., YAMADA C. and OHTANI S., *Surf. Sci.*, **601** (2007) 723.
- [6] TONA M., FUJITA Y., YAMADA C. and OHTANI S., *Phys. Rev B*, **77** (2008) 155427.
- [7] RITTER R., KOWARIK G., MEISSL W., SUSS L., MAUNOURY L., LEBIUS H., DUFOUR C., TOULEMONDE M. and AUMAYR F., *Nucl. Instrum. Methods Phys. Res. B*, **268** (2010) 2897.
- [8] RITTER R., KOWARIK G., MEISSL W., EL-SAID A. S., MAUNOURY L., LEBIUS H., DUFOUR C., TOULEMONDE M. and AUMAYR F., *Vacuum*, **84** (2010) 1062.
- [9] BOUFFARD S., COUSTY J., PENNEC Y. and THIBAUDAU F., *Radiat. Eff. Defects Solids*, **126** (1993) 225.
- [10] CHADDETON L. T., *Radiat. Meas.*, **36** (2003) 13.
- [11] KHALFAOUI N., ROTARU C. C., BOUFFARD S., TOULEMONDE M., STOQUERT J. P., HAAS F., TRAUTMANN C., JENSEN J. and DUNLOP A., *Nucl. Instrum. Methods Phys. Res. B*, **240** (2005) 819.
- [12] TRAUTMANN C., TOULEMONDE M., COSTANTINI J. M., GROB J. J. and SCHWARTZ K., *Phys. Rev B*, **62** (2000) 13.
- [13] GONIN Y., MUNNIK F., BENNINGER F. and MIKHAILOV S., *Appl. Surf. Sci.*, **217** (2003) 289.
- [14] VAN KAN J., BETTIOL A. and WATT F., *Appl. Phys. Lett.*, **83** (2003) 1629.
- [15] KUBENA R., WARD J., STRATTON F., JOYCE R. and ATKINSON G., *J. Vac. Sci. Technol. B*, **9** (1991) 3079.
- [16] ALVES A., JOHNSTON P. N., REICHART P., JAMIESON D. N. and SIEGELE R., *Nucl. Instrum. Methods Phys. Res. B*, **260** (2007) 431.
- [17] DOBELI M., AMES F., MUSIL C. R., SCANDELLA L., SUTER M. and SYNAL H. A., *Nucl. Instrum. Methods Phys. Res. B*, **143** (1998) 503.
- [18] PAPALEO R., SILVA M., LEAL R., GRANDE P., ROTH M., SCHATAT B. and SCHIWIETZ G., *Phys. Rev. Lett.*, **101** (2008) 167601.
- [19] KALESS A., SCHULZ U., MUNZERT P. and KAISER N., *Surf. Coat Technol.*, **200** (2005) 58.
- [20] KONDYURIN A. and BILEK M., *Nucl. Instrum. Methods Phys. Res. B*, **269** (2011) 1361.
- [21] VOURDAS N., TSEREPI A. and GOGOLIDES E., *Nanotechnology*, **18** (2007) 125304.
- [22] GILLASPY J., PARKS D. and RATLIFF L., *J. Vac. Sci. Technol. B*, **16** (1998) 3294.
- [23] ZSCHORNACK G., GROSSMANN F., HELLER R., KENTSCH U., KRELLER M., LANDGRAF S., OVSYANNIKOV V. P., SCHMIDT M. and ULLMANN F., *Nucl. Instrum. Methods Phys. Res. B*, **258** (2007) 205.
- [24] LOPEZ-URRUTIA J., DORN A., MOSHAMMER R. and ULLRICH J., *Phys. Scr.*, **1999** (1999) 502.
- [25] GINZEL R., HIGGINS S. G., MROWCYNKI P., NORTHWAY P., SIMON M. C., TAWARA H., LOPEZ-URRUTIA J. R.

- C., ULLRICH J., KOWARIK G., RITTER R., MEISSL W., VASKO C., GOESSELSBERGER C., EL-SAID A. S. and AUMAYR F., *Nucl. Instrum. Methods Phys. Res. B*, **268** (2010) 2972.
- [26] HORCAS I., FERNANDEZ R., GOMEZ-RODRIGUEZ J., COLCHERO J., GOMEZ-HERRERO J. and BARO A., *Rev. Sci. Instrum.*, **78** (2007) 013705.
- [27] PIGNATARO B., FRAGALA M. and PUGLISI O., *Nucl. Instrum. Methods Phys. Res. B*, **131** (1997) 141.
- [28] ARNAU A., AUMAYR F., ECHENIQUE P. M., GREYER M., HEILAND W., LIMBURG J., MORGENSTERN R., RONCIN P., SCHIPPERS S., SCHUCH R., STOLTERFOHT N., VARGA P., ZOUROS T. J. M. and WINTER H. P., *Surf. Sci. Rep.*, **27** (1997) 117.
- [29] SCHENKEL T., HAMZA A. V., BARNES A. V. and SCHNEIDER D. H., *Progr. Surf. Sci.*, **61** (1999) 23.
- [30] WINTER H. P. and AUMAYR F., *J. Phys. B: At. Mol. Opt. Phys.*, **32** (1999) R39.
- [31] AUMAYR F. and WINTER H. P., *Philos. Trans. R. Soc. London, Ser. A*, **362** (2004) 77.
- [32] AUMAYR F. and WINTER H. P., *Springer Tracts Mod. Phys.*, **225** (2007) 79.
- [33] MEISSL W., WINKLEHNER D., AUMAYR F., SIMON M. C., GINZEL R., CRESPO LÓPEZ-URRUTIA J. R., ULLRICH J., SOLLEDER B., LEMELL C. and BURGDÖRFER J., *e-J. Surf. Sci. Nanotechnol.*, **6** (2008) 54.
- [34] EL-SAID A. S., HELLER R., AUMAYR F. and FACSKO S., *Phys. Rev. B*, **82** (2010) 033403.